Indirectly pumped 3.7 THz InGaAs/InAlAs quantum-cascade lasers grown by metal-organic vapor-phase epitaxy

Kazuue Fujita,[1] Masamichi Yamanishi,[1,*] Shinichi Furuta,[1] Kazunori Tanaka,[1] Tadataka Edamura,[1] Tillmann Kubis,[2] and Gerhard Klimeck[2]

[1]*Central Research Laboratories, Hamamatsu Photonics K.K. Hamakitaku, Hamamatsu, 434-8601, Japan*
[2]*Network for Computational Nanotechnology, Birck Nanotechnology Center, Purdue University, W. Lafayette, Indiana 47907, USA*
[*]*masamiya@crl.hpk.co.jp*

Abstract: Device-performances of 3.7 THz indirect-pumping quantum-cascade lasers are demonstrated in an InGaAs/InAlAs material system grown by metal-organic vapor-phase epitaxy. The lasers show a low threshold-current-density of ~420 A/cm^2 and a peak output power of ~8 mW at 7 K, no sign of parasitic currents with recourse to well-designed coupled-well injectors in the indirect pump scheme, and a maximum operating temperature of T_{max}~100 K. The observed roll-over of output intensities in current ranges below maximum currents and limitation of T_{max} are discussed with a model for electron-gas heating in injectors. Possible ways toward elevation of T_{max} are suggested.

©2012 Optical Society of America

OCIS codes: (140.3070) Infrared and far-infrared lasers; (140.5965) Semiconductor lasers, quantum cascade; (230.5590) Quantum-well devices.

References and links

1. R. Köhler, A. Tredicucci, F. Beltram, H. E. Beere, E. H. Linfield, A. G. Davies, D. A. Ritchie, R. C. Iotti, and F. Rossi, "Terahertz semiconductor-heterostructure laser," Nature **417**(6885), 156–159 (2002).
2. B. S. Williams, "Terahertz quantum-cascade lasers," Nat. Photonics **1**(9), 517–525 (2007) (and references cited therein).
3. M. A. Belkin, J. A. Fan, S. Hormoz, F. Capasso, S. P. Khanna, M. Lachab, A. G. Davies, and E. H. Linfield, "Terahertz quantum cascade lasers with copper metal-metal waveguides operating up to 178 K," Opt. Express **16**(5), 3242–3248 (2008).
4. S. Kumar, Q. Hu, and J. L. Reno, "186 K operation of terahertz quantum-cascade lasers based on a diagonal design," Appl. Phys. Lett. **94**(13), 131105 (2009).
5. S. Fathololoumi, E. Dupont, C. W. Chan, Z. R. Wasilewski, S. R. Laframboise, D. Ban, A. Mátyás, C. Jirauschek, Q. Hu, and H. C. Liu, "Terahertz quantum cascade lasers operating up to ~ 200 K with optimized oscillator strength and improved injection tunneling," Opt. Express **20**(4), 3866–3876 (2012).
6. M. Fischer, G. Scalari, K. Celebi, M. Amanti, C. Walther, M. Beck, and J. Faist, "Scattering processes interahertz InGaAs/InAlAs quantum cascade lasers," Appl. Phys. Lett. **97**(22), 221114 (2010).
7. M. Tonouchi, "Cutting-edge terahertz technology," Nat. Photonics **1**(2), 97–105 (2007).
8. M. Yamanishi, K. Fujita, T. Edamura, and H. Kan, "Indirect pump scheme for quantum cascade lasers: dynamics of electron-transport and very high T_0-values," Opt. Express **16**(25), 20748–20758 (2008).
9. K. Fujita, M. Yamanishi, T. Edamura, A. Sugiyama, and S. Furuta, "Extremely high T_0-values (~450 K) of long-wavelength (~15 µm), low-threshold-current density quantum-cascade lasers based on the indirect pump scheme," Appl. Phys. Lett. **97**(20), 201109 (2010).
10. H. Yasuda, T. Kubis, P. Vogl, N. Sekine, I. Hosako, and K. Hirakawa, "Nonequilibrium Green's function calculation for four-level scheme terahertz quantum cascade lasers," Appl. Phys. Lett. **94**(15), 151109 (2009).
11. A. Wacker, "Extraction-controlled quantum cascade lasers," Appl. Phys. Lett. **97**(8), 081105 (2010).
12. T. Kubis, S. R. Mehrotra, and G. Klimeck, "Design concepts of terahertz quantum cascade lasers: Proposal for terahertz laser efficiency improvements," Appl. Phys. Lett. **97**(26), 261106 (2010).
13. S. Kumar, C. W. I. Chan, Q. Hu, and J. L. Reno, "A 1.8-THz quntum cascade laser operating significantly above the temperature of $\hbar\omega/k_B$," Nat. Phys. **7**(2), 166–171 (2011).
14. M. Yamanishi, K. Fujita, T. Kubis, N. Yu, T. Edamura, K. Tanaka, G. Klimeck, and F. Capasso, "Indirect pumping operation of THz InGaAs/InAlAs quantum-cascade-lasers," paper presented at Eleventh International Conference on Intersubband Transitions in Quantum Wells, Badesi, Italy, 11–17, September 2011.

#172845 - $15.00 USD Received 18 Jul 2012; revised 10 Aug 2012; accepted 20 Aug 2012; published 23 Aug 2012

15. E. Dupont, S. Fathololoumi, Z. R. Wasilewski, G. Aers, S. R. Laframboise, M. Lindskog, S. G. Razavipour, A. Wacker, D. Ban, and H. C. Liu, “A phonon scattering assisted injection and extraction based terahertz quantum cascade laser,” J. Appl. Phys. **111**(7), 073111 (2012).
16. S. Fathololoumi, E. Dupont, Z. R. Wasilewski, G. Aers, S. R. Laframboise, S. G. Razavipour, M. Lindskog, A. Wacker, D. Ban, and H. C. Liu, “Terahertz quantum cascade lasers based on phonon scattering assisted injection and extraction,” paper presented at Conference on Lasers and Electro-Optics (CLEO 2012), CTh4N.4, San Jose, CA, USA, 6–11, May 2012.
17. M. S. Vitiello, G. Scamarcio, and V. Spagnolo, “Temperature dependence of thermal conductivity and boundary resistance in THz quantum cascade lasers,” IEEE J. Quantum Electron. **14**(2), 431–435 (2008).
18. S. Kumar and Q. Hu, “Coherence of resonant-tunneling transport in terahertz quantum-cascade lasers,” Phys. Rev. B **80**(24), 245316 (2009).
19. T. Kubis, C. Yeh, P. Vogl, A. Benz, G. Fasching, and C. Deutsch, “Theory of nonequilibrium quantum transport and energy dissipation in terahertz quantum cascade lasers,” Phys. Rev. B **79**(19), 195323 (2009).
20. T. C. Kubis, “Quantum Transport in semiconductor nanostructures,” in *Selected Topics of Semiconductor Physics and Technology* (Munich, Germany, 2009) vol. 114.
21. The energy-diffusion model has been recently proposed by one (MY) of the authors; M. Yamanishi, unpublished note (2012).
22. P. Harrison and R. W. Kelsall, “The relative importance of electron-electron and electron-phonon scattering in terahertz quantum cascade lasers,” Solid-State Electron. **42**(7-8), 1449–1451 (1998).
23. M. S. Vitiello, R. C. Iotti, F. Rossi, L. Mahler, A. Tredicucci, H. E. Beere, D. A. Ritchie, Q. Hu, and G. Scamarcio, “Non-equilibrium longitudinal and transverse optical phonons in terahertz quantum cascade lasers,” Appl. Phys. Lett. **100**(9), 091101 (2012).
24. M. S. Vitiello, G. Scamarcio, V. Spagnolo, B. S. Williams, S. Kumar, Q. Hu, and J. L. Reno, “Measurement of subband electronic temperatures and population inversion in THz quantum-cascade lasers,” Appl. Phys. Lett. **86**(11), 111115 (2005).
25. T. Liu, T. Kubis, Q. Jie Wang, and G. Klimeck, “Design of three-well indirect pumping terahertz quantum cascade lasers for high optical gain based on noequilibrium Green’s function analysis,” Appl. Phys. Lett. **100**(12), 122110 (2012).

1. Introduction

Since the first demonstration of terahertz (THz) quantum-cascade lasers (QCLs) in 2001 [1], the device performances of THz QCLs have been remarkably improved. As a consequence of trials based on a variety of active/injector and waveguide structures [2], high temperature THz QCLs are mostly designed using resonant tunneling-based injection (direct pumping) and extraction of electrons from the lasing states in a GaAs/$Al_{0.15}Ga_{0.85}As$ material system with double metal waveguides [2–5]. The maximum operating temperature (T_{max}) of these THz QCLs has recently reached 199.5 K [5]. A 3.1 THz direct pumping InGaAs/InAlAs QCL of which layered structure grown by molecular beam epitaxy also exhibited a low threshold current density of ~200 A/cm^2, a peak output power of ~20 mW at 10 K but a relatively low T_{max} of ~122 K [6]. Obviously, device operation in a higher temperature range (≥250 K) which is achievable with a thermo-electric cooler would lead to a variety of applications of THz QCLs to pharmacology, non-invasive cross sectional imaging, quality control, gas and pollution sensing, biochemical label-free sensing, and security screening [7]. Yamanishi et al. [8] proposed a way to elevate T_{max} through an alternative pump scheme named indirect pump (IDP) scheme. This new approach has received a lot of attention since it can overcome, in principle, the 50% limitation of population-inversion in direct pump QCLs and, in turn result in a lower electron concentration in injector states [8]. The lower electron concentration would result in a reduced backfilling of electrons to lower laser states as well as a lower optical absorption in the injector. Both of these process improvements elevate the characteristic temperature (T_0) of threshold. The elevation of T_0 was, in fact, exhibited with mid-infrared IDP QCLs of a strong coupling between injector and IDP states above room temperature [8] [9]. Yasuda et al. [10], Wacker [11], and Kubis et al. [12] have examined theoretically a family of designs for THz IDP QCLs. Kumar et al. [13] have demonstrated a four well GaAs/$Al_{0.15}Ga_{0.85}As$ IDP-QCL at 1.8 THz with T_{max}~163 K, which surpasses the empirical relation, T_{max}≤(photon energy)/k_B. An IDP QCL consisting of active layers and coupled-well injectors has been also demonstrated at 4 THz with T_{max}~47 K, but with no considerable parasitic currents in a lattice-matched InGaAs/InAlAs material system grown by molecular beam epitaxy (MBE) [14]. Moreover, 3.2 THz GaAs/$Al_{0.25}Ga_{0.75}As$ IDP QCLs designed to fulfill “complete thermalization condition” proposed by Kubis et al. [12] have

#172845 - $15.00 USD Received 18 Jul 2012; revised 10 Aug 2012; accepted 20 Aug 2012; published 23 Aug 2012
(C) 2012 OSA

been recently exhibited with T_{max}~138 K [15] and T_{max}~144 K [16] but with relatively weak lasing.

In this work, we focus on laser performances of 3.7 THz IDP QCLs in the lattice-matched InGaAs/InAlAs material system grown by metal-organic vapor-phase epitaxy (MOVPE), showing a low threshold current density of ~420 A/cm^2 at 7 K, no sign of parasitic currents, and T_{max}~100 K. This is the first trial of laser action in THz InGaAs/InAlAs QCLs grown by MOVPE. The observed degradation of the laser performances such as roll-over of output intensities in current ranges below maximum currents and associated limitation of T_{max} will be discussed with a model for electron-gas heating caused by excess energies of electron systems in injectors. Possible ways toward elevation of T_{max} will be suggested.

2. Design of active/injector structures

Two types, A and B of active/injector structures were designed, as shown in Figs. 1(a) and 1(b), to incorporate the intermediate state, level 4 for the IDP process and to avoid coupling of the injector states, level 1′ with the adjacent upper and lower laser states, levels 3 and 2 under any bias fields. The decoupling of the injector states and states 2 and 3 is maintainable when the IDP scheme is adopted. This also enabled an efficient suppression of parasitic currents to negligible levels, despite the fact that injector and IDP states are strongly coupled with an anti-crossing gap $2\hbar\Omega_{1'4}$~4 meV (see the next section). The relaxation times due to LO-phonon emissions and elastic scatterings by interface roughness and alloy disorder are estimated: τ_{43} ~0.5 ps, τ_{42}~8.5 ps, $\tau_{42'}$~24 ps, and τ_3 ~1.6 ps for a type-A QCL, and τ_{43} ~0.5 ps, τ_{42}~9.9 ps, $\tau_{42'}$~22 ps, and τ_3 ~2.1 ps for a type-B QCL. The resulting pump efficiencies, $\eta_{pump} = (1/\tau_{43})/[(1/\tau_{43}) + (1/\tau_{42}) + (1/\tau_{42'})]$, are high enough ($\eta_{pump}$~0.88 for the type-A QCL and η_{pump}~0.92 for the type-B QCL). The resulting transition dipole moment is also large enough (Z_{32}~4.3 nm) for both QCL types. The energy between the IDP and upper laser states has a common value, i.e. E_{43}~34 meV which equals the averaged LO-phonon energy E_{LO} in InGaAs

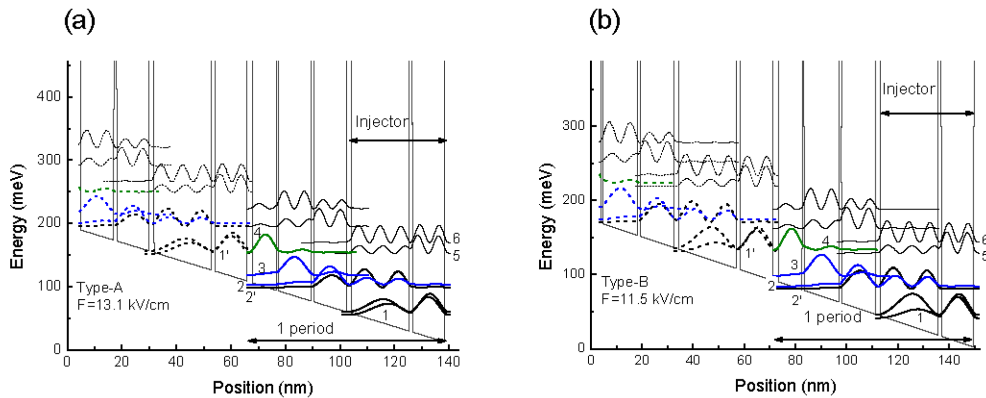

Fig. 1. Conduction band diagrams and moduli squared of the relevant wavefunctions in the designed active/injector regions of type-A and -B THz IDP QCLs. The lattice-matched $In_{0.53}Ga_{0.47}As/In_{0.52}Al_{0.48}As$ layer sequences of one period of the active/injector layers, in angstroms, starting from the injection barrier (toward the right side) are as follows: (a) **20**/89/**7**/121/**10**/119/**18**/210/**14**/118 and (b) **22**/93/**7**/137/**9**/133/**18**/225/**14**/127 where $In_{0.52}Al_{0.48}As$ barrier layers are in bold and $In_{0.53}Ga_{0.47}As$ QW layers in roman, and Si-donors are quasi-δ-doped in the underlined layers. The bias fields are assumed to be high enough, (a) 13.1 kV/cm and (b) 11.5 kV/cm, to almost align the ground state 1′ of the injector to the IDP state, level 4.

while the difference between the lower laser and injector states is designed to have two different values, namely E_{21}~40 meV for type-A and E_{21}~35 meV for type-B. These energy differences guarantee fast depopulation of the lower laser states, τ_{21}<0.5 ps<<τ_3, in contrast to

#172845 - $15.00 USD Received 18 Jul 2012; revised 10 Aug 2012; accepted 20 Aug 2012; published 23 Aug 2012
(C) 2012 OSA

the case of references [15, 16]. In these references, the separation is designed to be 9-meV lower than the LO-phonon energy in GaAs to fulfill the thermalization condition. The lower energy separation however was found in the same references to lead to weaker lasing. The energy separation between the upper and lower laser states is designed to be E_{32}~15 meV for both the types of QCLs.

3. Device performances

The designed structures, depicted in Figs. 1(a) and 1(b), with an injector Si doping of ~2 × 10^{10} cm^{-2} per module and with 140 and 128 repetitions for the type-A and -B devices, respectively were grown on InP substrates by MOVPE to obtain 10-µm-thick active regions. The active regions were sandwiched between 100-nm and 75-nm thick n^+-InGaAs layers on which good ohmic contacts are easily obtainable unlike GaAs layers. The wafers were processed into THz QCL structures with Ti/Au double metal waveguides. The ridge width of the waveguides is ~130 µm and the length of the Fabry-Perot resonators ~1.5 mm. The output powers were detected by using a high-resistivity Si hyper-hemispherical lens with a diameter of 12 mm adjacent to laser chips and a calibrated thermo-pile detector (3A-P-THz, Ophir Photonics).

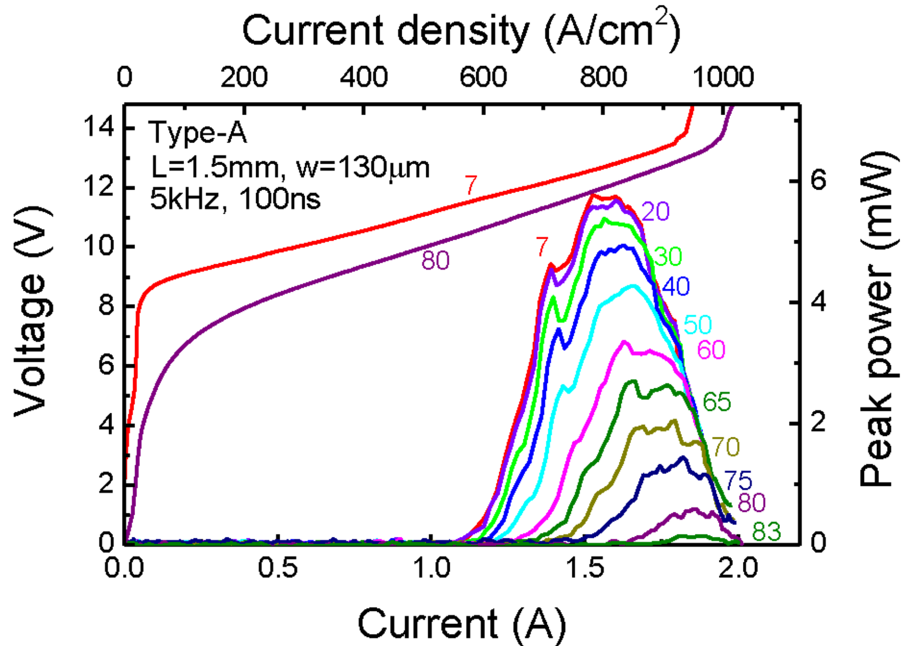

Fig. 2. Light intensity-voltage-current (current density) characteristics of a type-A IDP QCL at different temperatures, 7 K–83 K.

Figure 2 shows the light (*L*)-voltage (*V*)-current (*I*) (or –current density (*J*)) characteristics of a type-A QCL in the temperature range of 7 K to 83 K in pulsed mode with a pulse width of 100 ns and a repetition rate of 5 kHz. The IDP laser exhibits a low threshold current density of ~550 A/cm^2 with a reasonably wide dynamic range of 550 A/cm^2 to 900 A/cm^2 at temperatures of 7 to 30 K, despite the relatively small number of cascade modules of 140. The *V–I* curves of the present IDP laser indicate a continuous resonant tunneling to the intermediate state, level 4 over the entire current range. In spite of the strong coupling $2\hbar\Omega_{1'4}$~4 meV, there is no significant sign of resonant tunneling to the lower levels 2 and 3 which is very different to conventional direct pump THz QCLs [2–5] and, also different to previously reported THz IDP QCLs [15, 16]. The peak output power is obtained to be high ~6 mW at 7 K. Obviously, the laser performance of the present MOVPE-grown device is

#172845 - $15.00 USD Received 18 Jul 2012; revised 10 Aug 2012; accepted 20 Aug 2012; published 23 Aug 2012
(C) 2012 OSA

substantially better than that (T_{max}~47 K) of our previous MBE-grown device [14]. Both devices were based on the same active/injector structure design. However, it is difficult to keep the thicknesses of well and barrier layers constant during the many hours long MBE growth. These quality issues are avoided in the MOVPE growth.

Figure 3 depicts *L-V-I (J)* characteristics of a type-B QCL in the temperature range of 7 K to 100 K and in the same pulsed mode as described above. It shows a lower threshold current density of ~420 A/cm^2 at 7 K and a higher T_{max} of ~100 K, despite the fact that a smaller number of modules (128) were grown than in the type A QCL. The threshold current density, J_{th}~420 A/cm^2 at 7 K is substantially lower than previously reported ones (J_{th}~900 A/cm^2 in the 1.8 THz GaAs/$Al_{0.15}Ga_{0.85}As$ IDP-QCL at 10 K of Ref [13]. and J_{th}~900 A/cm^2 in the 3.2 THz GaAs/$Al_{0.25}Ga_{0.75}As$ IDP-QCL at 10 K of Ref [16].). The peak output powers are obtained to be even higher, ~8 mW at 7 K and ~4.3 mW at 80 K, compared to those of the type-A device. It should be stressed that there is no indication for parasitic currents due to resonant tunneling to levels 2 and 3 at 7 K and 80 K in the *V-I* characteristics of both QCL types. This favorable fact can be understood in the band diagram shown in the insertion of Fig. 3. For a low bias field of ~3.5 kV/cm, the ground state level 1′ of the coupled-well injector of the previous period is located far away from levels 2 and 3. Parasitic currents are completely suppressed, since the second state level 1″ is strongly coupled with level 4 which causes most

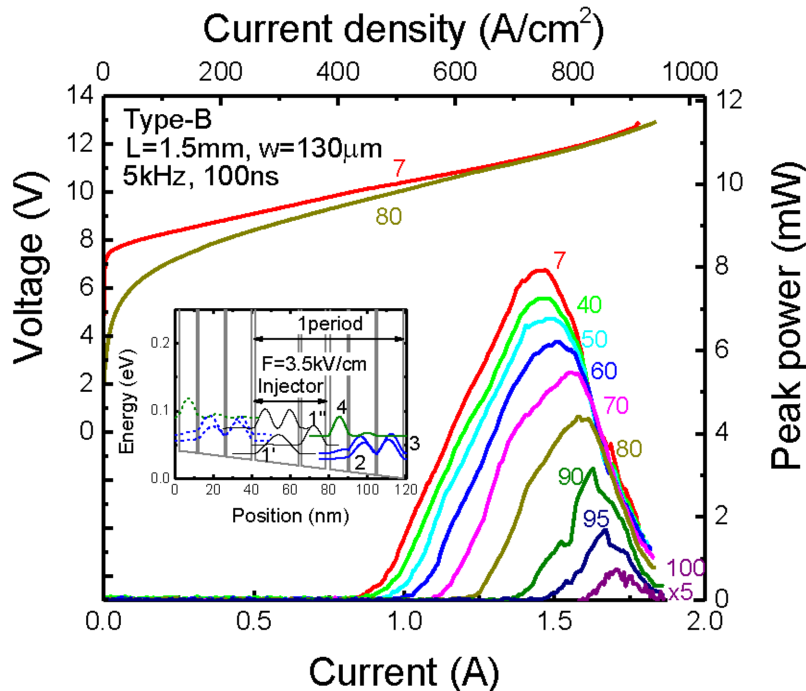

Fig. 3. Light intensity-voltage-current (current density) characteristics of a type-B IDP QCL at different temperatures, 7 K-100 K. The insertion shows the band diagram and moduli squared of the relevant wavefunctions in the active/injector regions of the type-B QCL biased by a low electric field of ~3.5 kV/cm.

of the current density at a higher temperature ~80 K which is shown in Fig. 3. This is very much different to the *V-I* characteristics of 3.2 THz four-well design GaAs/$Al_{0.25}Ga_{0.75}As$ IDP QCLs [15,16] in which at low bias fields the upper and lower laser-states, 3 and 2 are designed to be spatially closer to the injector state 1′, resulting in substantial parasitic currents. It is to be noted that the current-turn-on voltage ~8 V is linked to the alignment of

#172845 - $15.00 USD Received 18 Jul 2012; revised 10 Aug 2012; accepted 20 Aug 2012; published 23 Aug 2012
(C) 2012 OSA

level 1′ with level 4. However, the *L-I* curves of both the types of present QCLs exhibit serious roll-over of light output in the current ranges below the maximum currents. In the next section, theoretical results on electron transport in the active/injector structures are shown that explain the origin of this roll-over. The measured emission spectra for both the types of QCLs at different biases are displayed in Fig. 4. It shows a blue-shift with increasing bias current (voltage). This blue shift of the emission spectra indicates that the lasing in the IDP QCLs indeed originate from diagonal transitions between the upper and lower laser levels 3 and 2 in

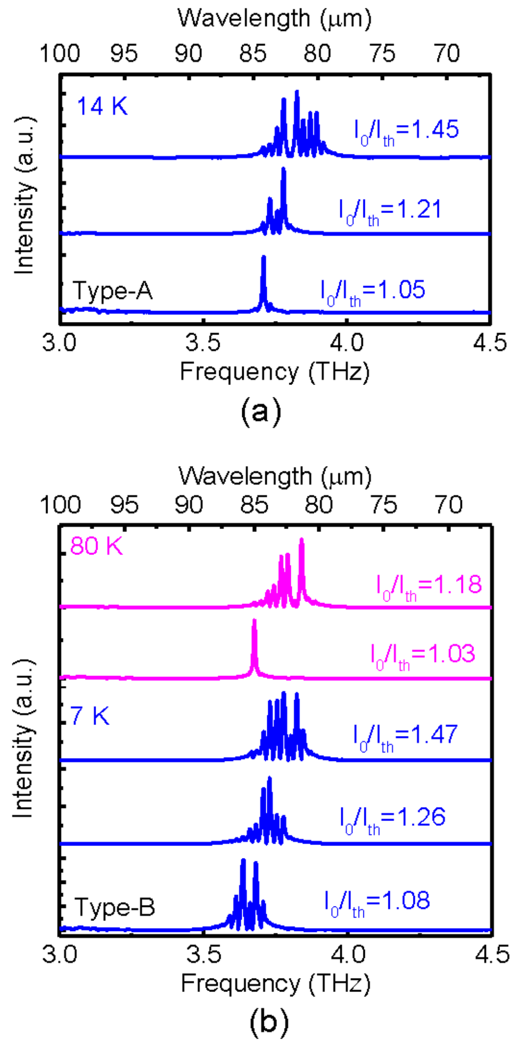

Fig. 4. THz spectra emitted from (a) the type-A and (b) type-B QCLs for different biases at temperatures, 14 K, and 7 K and 80 K, respectively.

the entire current range. The laser was tested in higher duty cycle pulse mode but it ceased lasing at a heat sink temperature of 80 K in 10% duty cycle driving. This seems to be caused by a serious temperature rise in the active region due to a high Kapitza or thermal boundary resistance in the InGaAs/AlInAs layered structure [17].

Figure 5 depicts the observed differential resistance R_d as functions of injection current in a direct pump QCL and both types A and B of IDP QCLs. The discontinuities of R_d at threshold current densities were observed to be ~42% with the direct pump QCL and ~20% with the type-A and ~25% with the type-B QCL. The more shallow depths of R_d in the case of

#172845 - $15.00 USD Received 18 Jul 2012; revised 10 Aug 2012; accepted 20 Aug 2012; published 23 Aug 2012
(C) 2012 OSA

the IDP QCLs (about half of the one in the direct pump QCL) are quite consistent with previously published theoretical results in the fast depopulation condition $\tau_{21} \ll \tau_3$ [15, 18]. This difference in the R_d-discontinuities originates from a different amount of clamping of the state populations that are relevant for tunneling through the injection barriers above thresholds. It is to be noticed that the upper laser states of IDP QCLs are not relevant for the tunneling process though their electron populations above thresholds are well-clamped in the condition $\tau_{21} \ll \tau_3$ and the smaller R_d-discontinuities of the IDP QCLs compared with that of the DP QCL do not necessarily mean lower quantum efficiencies of the IDP QCLs. The clear discontinuities, obviously, reveal that stronger lasing took place in the present IDP QCLs compared to references [15, 16]. Moreover, the differential resistance in the direct pump QCL is peaked at a current of ~0.5 A below threshold current. This is caused by current switching from parasitic to main one. On the other hand, the R_d-curves for the IDP QCLs are flat in the same current range. The latter indicates the absence of parasitic currents below threshold.

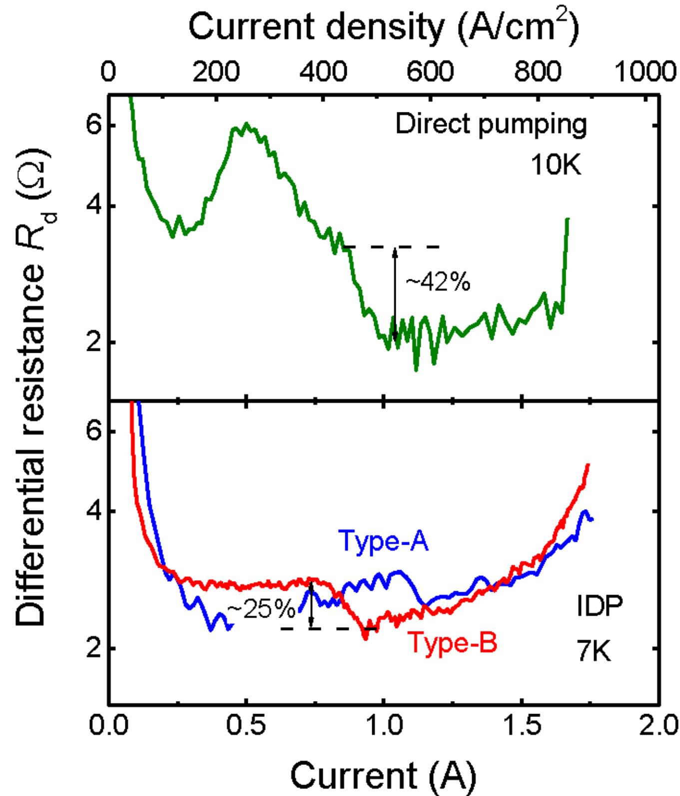

Fig. 5. Differential resistance R_d in logarithmic scale as functions of current in a direct pump InGaAs/InAlAs QCL at 10 K, and the type-A and –B IDP QCLs at 7 K.

4. Simulations and discussion

We have carried out simulations on electron transport in the active/injector region of the present IDP QCLs, based on nonequilibrium Green's function (NEGF) formalism [19,20]. In the NEGF analysis, the electron-electron interaction was taken into account within the mean-field Hartree approximation. Figure 6 shows the calculated spectral function (effective density-of-states) at vanishing in-plane momentum $k_{//} = 0$ (contour lines) and energy resolved current density (colored contour plot) in the first module of the type-A QCL. Obviously, electrons of the IDP level 4 scatter into the upper laser level 3 by resonantly emitting LO-phonons. Hereby, no leakage to spurious levels 5 and 6 is observed. In the widest quantum

#172845 - $15.00 USD Received 18 Jul 2012; revised 10 Aug 2012; accepted 20 Aug 2012; published 23 Aug 2012
(C) 2012 OSA

well, the electrons emit another LO-phonon and scatter into level 1 with a large kinetic energy of ~30 meV (excess energy $E_{excess} = E_{41}–2E_{LO}$). Due to efficient coherent tunneling, these highly nonequilibrium electrons tend to be directly transferred to the IDP subband of the next module. The reduction of the excess energy even in IDP QCLs is important for avoiding electron-gas heating as pointed out in reference [12]. However, in the present simulation, influences of the numerically very demanding higher order inelastic electron-electron (*e-e*) scattering that might thermalize portions of these electrons is neglected. Note that the assumed electron distribution in the IDP subband of the QCL period in Fig. 6 is well thermalized. Additional heuristic discussions on the impact of the inelastic *e-e* scatterings will be done below.

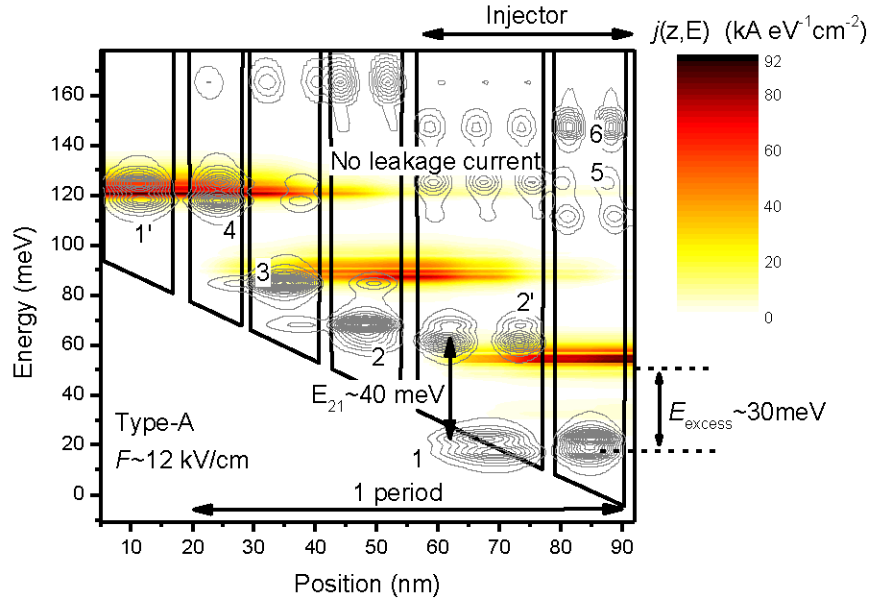

Fig. 6. Computed spectral functions (contour lines) at $k_{//} = 0$ and energy-resolved current densities (colored areas) in the first module of the type-A QCL at 40 K. The simulation was carried out, based on the NEGF formalism, assuming the mean-field approximation for electron-electron interaction. In the simulation, we used an effective interface roughness height, Λ = 2.4 Å and a roughness correlation length, λ_c = 90 Å, and an alloy-scattering potential, δV_{alloy} = 0.6 eV, and, also, included phonon and impurity scattering. The bias field was assumed to be ~12 kV/cm.

#172845 - $15.00 USD Received 18 Jul 2012; revised 10 Aug 2012; accepted 20 Aug 2012; published 23 Aug 2012
(C) 2012 OSA

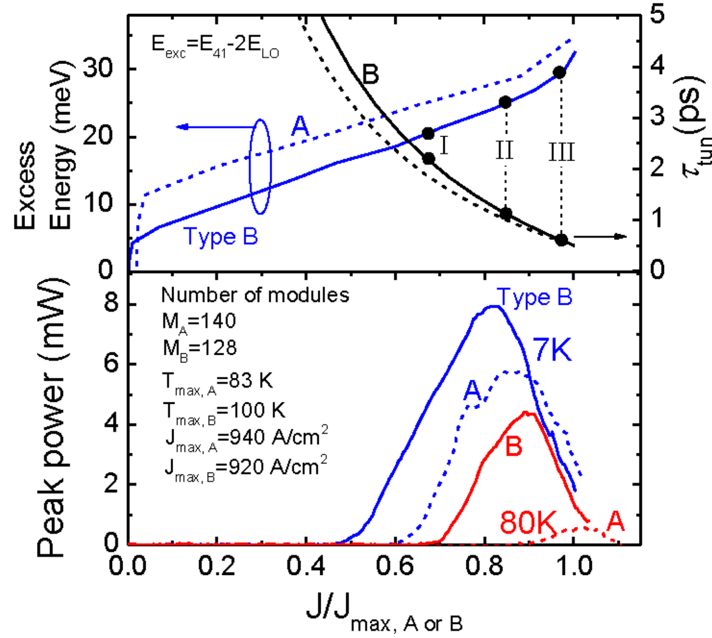

Fig. 7. Light intensity, estimated excess energy, and tunneling time as functions of normalized current $J/J_{\text{max, A or B}}$ for the type-A (dashed curves) and –B (solid curves) IDP QCLs. $J_{\text{max, A or B}}$ is the maximum current density at 7 K in the type-A or –B QCL.

Figure 7 shows the light output intensity, estimated excess energy E_{excess}, and tunneling time τ_{tun} as functions of the normalized current $J/J_{\text{max, A or B}}$ for both the types of QCLs. The excess energies $E_{\text{excess}} = E_{41}-2E_{\text{LO}}$ were estimated by solving Schrödinger/Poisson equations by assuming electric fields, induced by corresponding bias voltages in the *V-I* characteristics at 7 K. The tunneling times through injection barriers were estimated assuming the limit $\tau_{21} \ll \tau_{\text{relax}}$ and neglecting any back-scatterings [8]

$$\tau_{\text{tun}}/\tau_{\text{tun},0} = J_{\max}/J + \left[J_{\max}/J - 1\right]\left(\tau_{\text{relax}}/\tau_{\text{tun},0}\right), \quad (1)$$

where $\tau_{\text{relax}} = \eta_{\text{pump}}(\tau_3 + 2\tau_{43})$ is the global relaxation time, 2.3 ps for the type-A or 2.85 ps for the type-B QCL, and the on-resonant tunneling time through injection barriers at a maximum current is given by $\tau_{\text{tun},0} = 1/2\Omega_{1'4}^2\tau_{\text{deph}}$ (~0.5 ps in the present cases) with the dephasing time, τ_{deph}~100 fs. The better laser performance, such as lower threshold, higher output, and higher $T_{\max}$ of the type-B QCL would be ascribable partly to the slightly larger η_{pump}~0.92 and slightly longer τ_3~2.1 ps but also to the 5-meV lower excess energies. However, the excess energy increases proportionally with increasing current while the roll-over of output intensities takes place sharply in the current range below $J_{\max}$. Leakage currents cannot explain the roll-over since they are absent as shown in Fig. 6. Furthermore, the observed *V–I* characteristics shown in Figs. 2 and 3 and in the bottom of Fig. 5 show no sharp decrease of their slopes in current range of the roll-over which is very different to the findings of reference [13] (See the slope changes in high current ranges, ≥1200 A/cm^2 of the *V–I* curves in Fig. 4a of the reference).

The influence of inelastic *e-e* scatterings on the electron distribution in the injector subbands is important for the roll-over of the laser performance and the limitation of $T_{\max}$. To estimate the influence of this scattering mechanism, the electron distribution for different dwell times, i.e., different tunneling times based on the energy-diffusion model of Ref [21]. was considered. The key points of the energy-diffusion model are as follows: Given an intrasubband *e-e* scattering event in a quantum well, with a momentum transfer of $\boldsymbol{q}$, an

#172845 - $15.00 USD Received 18 Jul 2012; revised 10 Aug 2012; accepted 20 Aug 2012; published 23 Aug 2012
(C) 2012 OSA

electron with a momentum $\boldsymbol{k}$ loses a certain amount of energy whereas the other electron gains the same amount of energy. This energy transfer is represented by $\Delta E = (\hbar^2k^2/2\text{m}^*)\{-2(q/k)\cos\theta + (q/k)^2\}$ where θ is the angle between $\boldsymbol{k}$ and $\boldsymbol{q}$. Averaging the scattering angle, $\pi/2<\theta<3\pi/2$ (energy gain) or $-\pi/2<\theta<\pi/2$ (energy loss), the averaged energy transfer is given by $<\Delta E>_{\text{av}} = (\hbar^2k^2/2\text{m}^*)\{\pm(4/\pi)(q/k) + (q/k)^2\}$. In general, the *e-e* scattering potential decreases sharply with increasing momentum transfer q if q is larger than the inverse screening length (S~2×10^5 1/cm)

$$V(q)^2 \propto \left|\iint \mathrm{d}z\mathrm{d}z'\Psi(z)^2\Psi(z')^2\exp[-Q\,|z-z'|]\right|^2 \Big/ Q^2, \tag{2}$$

in which $Q^2 = q^2 + S^2$ and $\Psi(z)$ is the wavefunction in a subband. The average momentum transfer becomes q_{av}~S and the average energy transfer becomes $<\Delta E>_{\text{av}}\sim\pm(4/\pi)(\hbar^2kS/2\text{m}^*)$ when S is much smaller than the considered electron momenta. Thus, one may view the *e-e* scattering process as a kind of diffusion process in energy space. Then, the energy-diffusion coefficient is given by $D_{\text{e}} = \{<\Delta E>_{\text{av}}/\tau_{\text{e-e}}\}^2\tau_{\text{e-e}} = \{<\Delta E>_{\text{av}}\}^2/\tau_{\text{e-e}}$, where $\tau_{\text{e-e}}$, the intrasubband *e-e* scattering time is typically ~100 fs [22]. Phenomenological relations between the *e-e* (diffusion model) and LO-phonon scattering mechanisms were applied for non-degenerate electron system in steady-state and with boundary conditions $\mathrm{d}n(E)/\mathrm{d}E = 0$ at the subband edge $E = 0$ and $n(E)\rightarrow0$ for $E\rightarrow\infty$, were used to calculate the energy-resolved electron population $n(E)$; for $E<E_{\text{LO}}$

$$g(E)+D_{\text{e}}\mathrm{d}^2n(E)/\mathrm{d}E^2-n(E)[N_{\text{phonon}}/\tau_{\text{LO}}]+n(E+E_{\text{LO}})\left[\left(1+N_{\text{phonon}}\right)/\tau_{\text{LO}}\right]-n(E)/\tau_{\text{tun}}=0, \tag{3}$$

and for $E>E_{\text{LO}}$

$$\begin{aligned} g(E)+D_{\text{e}}\mathrm{d}^2n(E)/\mathrm{d}E^2-\left[n(E)-n(E-E_{\text{LO}})\right]\left[N_{\text{phonon}}/\tau_{\text{LO}}\right] \\ +\left[n(E+E_{\text{LO}})-n(E)\right]\left[\left(1+N_{\text{phonon}}\right)/\tau_{\text{LO}}\right]-n(E)/\tau_{\text{tun}}=0, \end{aligned} \tag{4}$$

in which $g(E)$ is the generation rate, N_{phonon} the LO-phonon population, τ_{LO} the relaxation time due to LO-phonon spontaneous emissions, and τ_{tun} the escaping (tunneling) time. Here, it should be noted that the energy-diffusion model is not applicable to well-thermalized electron systems but to highly nonequilibrium electron systems like in the present case.

Figure 8 shows the calculated energy-resolved electron density of one effective injector subband of the first module for the three different conditions I (τ_{tun} = 2.1 ps and E_{excess} = 20 meV), II (τ_{tun} = 1.1 ps and E_{excess} = 25 meV), and III (τ_{tun} = 0.5 ps and E_{excess} = 30 meV). These conditions correspond to those bias points I, II, and III of the type-B QCL in Fig. 7. In the computation, the LO-phonon population was assumed to be small, $N_{\text{phonon}} = 6\times10^{-3}$, but the electron-population distributions were also confirmed to be quite similar even for a much larger N_{phonon}~0.4 [23] identified in the lasing condition of a direct pump THz-QCL. As shown in the middle figure, II of Fig. 8, e-e scattering tends to smear out the electron distribution and, consequently, electrons with high kinetic energies ($>E_{\text{LO}}$) relax down around the bottom of the injector subband by LO-phonon emissions. The left figure, I of Fig. 8 depicts more substantial cooling of the electron gas that is caused resultantly by the larger energy diffusion range $(D_{\text{e}}\tau_{\text{tun}})^{1/2}$~16 meV and short relaxation time τ_{LO}~0.2 ps compared with the long dwell time, τ_{tun} = 2.1 ps. This is a reason why such serious roll-over in current ranges below the maximum current density does not show up in direct pump QCLs even with similar amount of excess energies.

#172845 - $15.00 USD Received 18 Jul 2012; revised 10 Aug 2012; accepted 20 Aug 2012; published 23 Aug 2012
(C) 2012 OSA

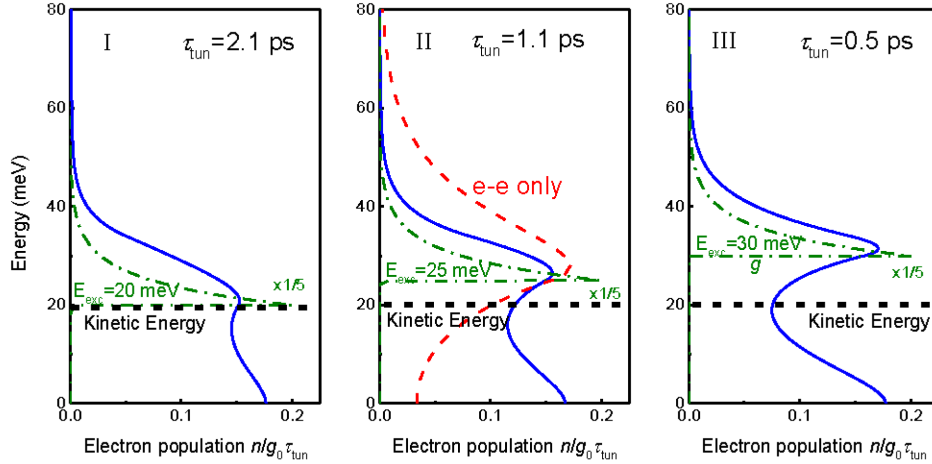

Fig. 8. Computed normalized energy-resolved electron populations, $n(E)/g_0\tau_{tun}$ (blue curves) for normalized generation spectra, $g(E)/g_0$ (dash-dotted green curves), where g_0 is the peak value of $g(E)$ in an injector subband of the first module for the bias conditions I (τ_{tun} = 2.1 ps and E_{excess} = 20 meV), II (τ_{tun} = 1.1 ps and E_{excess} = 25 meV), and III (τ_{tun} = 0.5 ps and E_{excess} = 30 meV). The calculated population distribution taking only into account the electron-electron scatterings is shown by the red dash-curve and is labeled with "*e-e* only". For reference, the initial kinetic energy, $E_{LO}–E_{32}$, required for thermally-activated-electron-LO-phonon relaxation in the upper laser subband in the next module is shown by the horizontal dashed lines. The computation was based on the energy-diffusion model. Hereby the parameters were D_e = 1.16 x 10^{14} $(\text{meV})^2$/s and τ_{LO} = 0.2 ps.

On-resonant tunneling times are designed to be long, $\tau_{tun,0} \geq 2$ ps due to weaker couplings, $2\hbar\Omega_{1'3} \leq 2$ meV for selective pumping of upper laser states in the direct pump QCLs. However, even with such long dwell-times, the electron population is not completely thermalized. This is causing increased electron temperature rises in upper laser subbands in direct pump THz QCLs as observed by Vitiello et al. [24]. In consecutive QCL modules, the electron-gas heating would build up periodically with a commensurability period that is larger than a single QCL period as pointed out in references [19, 20]. In particular, hot electrons of the upper laser levels of consecutive modules would thermalize via LO-phonon emissions which results in thermalized electron distributions in injector levels.

On the other hand, in the case of the right figure, III, a large fraction of electrons populate the range of kinetic energies higher than the minimum kinetic energy $E_{LO}–E_{32}$ (the horizontal dashed line) that is required to enable in the next module thermally-activated LO-phonon emissions from the upper laser subband. This implies that such hot carriers would be transferred through the IDP subband into the upper laser subband of the next module, while significantly reducing the population inversion. In conclusion, the roll-over of output intensities as well as the limitation of T_{max} are caused by highly nonequilibrium carriers in injector levels in the high current regime where the electronic dwell time is short. In other words, this problem can be solved by increasing the on-resonant tunneling time $\tau_{tun,0}$. However, the maximum tunneling time has to be limited by the global relaxation time $\eta_{pump}(\tau_3 + 2\tau_{43})$ to still benefit from the advantages of the IDP scheme and achieve a pronounced population-inversion as well as lower carrier-population in injector levels of the high current regime [8,9,25].

Another approach to eliminate the roll-over and increase T_{max} is to reduce the excess energy to the ultimate minimum value given by the photon energy. Lower photon energies (≤10 meV) lead to higher minimum kinetic energies, $E_{LO}–\hbar\omega_{opt}$ (≥24 meV) required for thermally-activated relaxation. It turns out that parasitic current densities that could pump lower laser levels are negligibly low even in THz (≤2.5 THz) IDP QCLs with such low emission frequencies. Another option for increasing T_{max} is the modified thermalization

#172845 - $15.00 USD Received 18 Jul 2012; revised 10 Aug 2012; accepted 20 Aug 2012; published 23 Aug 2012
(C) 2012 OSA

condition, that is, $E_{43}<E_{LO}$, $E_{31}>E_{LO}$, and $E_{41}\sim 2E_{LO}$ with $E_{21}\sim E_{LO}$ that would guarantee a fast depopulation from lower laser states [14]. It is worth to mention that the modified condition seemed to be satisfied incidentally around a bias field, ~15 kV/cm in the 1.8 THz IDP $GaAs/Al_{0.15}GaAs_{0.85}$ QCL of Ref [13]. which actually exhibited a high T_{max} of 163 K.

5. Conclusion

We have demonstrated device performances of 3.7 THz indirect-pumping MOVPE-grown InGaAs/InAlAs QCLs with two different energy separations between the lower laser level and the injector states, E_{21}~40 meV (type-A) and ~35 meV (type-B). Both lasers had Ti/Au double metal waveguides. Depending on the applied bias voltage, the type-B QCL has rather lower excess energies of ~20–30 meV. It exhibits a substantially better laser performance, a lower threshold current density of J_{th}~420 A/cm^2 at 7 K, a much higher peak output P_{peak}~4.3 mW at 80 K and a higher maximum operating temperature of T_{max}~100 K than the type-A QCL. Parasitic current densities associated with lower level pumping have been confirmed to be negligibly low in both the types of QCLs. However, both types of QCLs have shown serious roll-over of output intensities in current ranges below the maximum. According to theoretical analyses based on the NEGF formalism and the energy-diffusion model, the observed roll-over of output intensities and associated limitation of T_{max} have been ascribed to serious electron-gas heating caused by excess energies of the electrons. That is shown in the high current ranges in which tunneling times through the injection barriers reduce down to ~0.5 ps. Possible ways to avoid the roll-over and to increase T_{max} have been suggested. These suggestions include a slight increase of the on-resonant tunneling time, a reduction of the photon energy and/or the adoption of a modified condition for thermalization in THz IDP QCLs.

Acknowledgments

The authors at Hamamatsu Photonics K.K. acknowledge Doctor Kazuyoshi Kuroyanagi, Hamamatsu Photonics K.K. for his expertise in measurements of THz power. One (MY) of the authors expresses his thanks to Professor Supriyo Datta, Purdue University for insightful discussion particularly about the validity of the energy-diffusion model. The work at Hamamatsu Photonics K.K. has been, in part, supported by the Japan Society for the Promotion of Science (JSPS) through the "Funding Program for World-Leading Innovative R&D on Science and Technology (FIRST Program)," initiated by the Council for Science and Technology Policy (CSTP). Computational resources of nanoHUB.org and financial support by National Science Foundation under EEC-0228390 and OCI-0749140 were utilized in the NEGF analysis and are acknowledged.

#172845 - $15.00 USD Received 18 Jul 2012; revised 10 Aug 2012; accepted 20 Aug 2012; published 23 Aug 2012
(C) 2012 OSA